Heliyon 10 (2024) e34540

Contents lists available at ScienceDirect

Heliyon

journal homepage: www.cell.com/heliyon

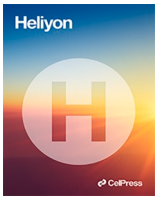

Research article

Synthesis, DFT, and *in silico* biological evaluation of chalcone bearing pyrazoline ring against *Helicobacter pylori* receptors

Najla A. Alshaye [a], Nuha Salamah Alharbi [b], Mohamed A. El-Atawy [c], Reham O. El-Zawawy [c,*], Ezzat A. Hamed [c], Mohammed Elhag [d], Hoda A. Ahmed [e], Alaa Z. Omar [d]

[a] *Department of Chemistry, College of Science, Princess Nourah bint Abdulrahman University, P.O. Box 84428, Riyadh, 11671, Saudi Arabia*
[b] *Chemistry Department, College of Science, Taibah University, Medina 30002, Saudi Arabia*
[c] *Chemistry Department, Faculty of Science, Alexandria University, Alexandria, 21231, Egypt*
[d] *Chemistry Department, Faculty of Science, Damanhour University, Damanhour, 22511, Egypt*
[e] *Department of Chemistry, Faculty of Science, Cairo University, Giza, 12613, Egypt*

ARTICLE INFO

Keywords:
Pyrazole
Chalcone
Molecular docking
DFT
Helicobacter pylori

ABSTRACT

Peptic ulcer disease (PUD), often caused by *Helicobacter pylori* infection, is a prevalent gastrointestinal condition characterized by the erosion of the gastric or duodenal mucosal lining. *H. pylori* adheres to gastric epithelial cells, secreting toxins and disrupting the stomach's defenses. *H. pylori* relies on various receptors to establish infection, making these molecules attractive therapeutic targets. This study aimed to develop novel anti-ulcer compounds by combining benzothiazole, pyrazoline, and chalcone pharmacophores. A series of chalcone derivatives **4a-c** were synthesized *via* Claisen-Schmidt condensation and characterized using spectroscopic techniques such as FT-IR, NMR and elemental analysis. The DFT calculations, using B3LYP method with 6-311G basis set, revealed the *p*-tolyl derivative **4b** exhibited the highest thermal stability while the *p*-bromophenyl derivative **4c** showed the lowest stability but highest chemical reactivity. The HOMO-LUMO energy gaps as well as the dipole moments decreased in the order: **4b** > **4a** > **4c**, reflecting a similar reactivity trend. Molecular docking showed ligands **4a-c** bound effectively to the *H. pylori* urease enzyme, with docking scores from −5.3862 to −5.7367 kcal/mol with superior affinity over lansoprazole. Key interactions involved hydrogen bonds and hydrophobic pi-hydrogen bonds with distances ranging 3.46–4.34 Å with active site residues ASN666, SER714 and ASN810. The combined anti-inflammatory, antimicrobial, and *H. pylori* anti-adhesion properties make these novel chalcones promising PUD therapeutic candidates.

1. Introduction

Peptic Ulcer Disease (PUD) is a prevalent gastrointestinal affliction, characterized by the erosion of the mucosal lining of the stomach or duodenum [1]. Annually, PUD affects around 4 million people worldwide [2], presenting symptoms such as abdominal pain, bloating, nausea, vomiting, and blood in stool [3]. Untreated ulcers can lead to severe internal bleeding and increase the risk of stomach cancer [4,5]. Among the various factors contributing to PUD, the bacterium *Helicobacter pylori* emerges as a pivotal player [6].

* Corresponding author.
E-mail addresses: naalshaye@pnu.edu.sa (N.A. Alshaye), Nssharbi@taibahu.edu.sa (N.S. Alharbi), alaazaki@alexu.edu.eg (R.O. El-Zawawy), ahoda@sci.cu.edu.eg (H.A. Ahmed).

https://doi.org/10.1016/j.heliyon.2024.e34540
Received 6 May 2024; Received in revised form 9 June 2024; Accepted 11 July 2024
Available online 14 July 2024

This microorganism colonizes the gastric mucosa, instigating inflammation and disrupting the delicate equilibrium of the stomach's microenvironment [7]. A key virulence factor of *H. pylori* is the urease enzyme [8,9] which catalyzes the hydrolysis of urea to ammonia and carbon dioxide, neutralizing the stomach's acidic environment and fostering bacterial survival [10,11].

H. pylori relies on a sophisticated set of receptors for successful colonization and evasion of host defenses. These receptors play a crucial role for adherence to gastric epithelial cells and facilitating the injection of bacterial toxins [12]. Of particular significance is the interaction between *H. pylori* and the host cell receptors s, influencing infection severity and persistence. The Lewis antigen system is a key recognition site for *H. pylori* adhesion [13]. Understanding these receptor interactions provides a unique avenue for therapeutic interventions, paving the way for novel compounds designed to disrupt bacterial adherence and infection establishment, Fig. 1.

Heterocyclic compounds have found extensive utility across diverse fields, serving as key building blocks in pharmaceuticals, agrochemicals, materials science, and beyond, owing to their versatile chemical properties and wide-ranging biological activities [14–16]. The benzothiazole ring possesses anti-inflammatory properties which play a crucial role in mitigating the inflammatory response associated with *H. pylori* infection [17,18]. Additionally, pyrazolines have exhibited significant antimicrobial activity [19,20], making them particularly relevant in addressing the bacterial colonization aspect of *H. pylori*, a major contributor to PUD pathogenesis [21]. This approach aims to capitalize on the anti-inflammatory and antimicrobial properties of the individual moieties, culminating in a compound with enhanced therapeutic potential against PUD. These modifications are intended to optimize the interaction of the compounds with *H. pylori* and enhance their affinity for specific molecular targets [22–24].

In silico biological evaluation, particularly through molecular docking studies, plays a pivotal role in early drug discovery for chalcone-bearing pyrazoline rings [25,26]. This approach allows researchers to predict the binding affinity and interactions of these compounds with target proteins before in vitro testing. By identifying promising candidates early on, *in silico* methods save time and resources, streamline experimental efforts, and guide the rational design of more effective derivatives.

This study endeavors to synthesize and characterize a series of novel compounds, combining benzothiazole, pyrazoline, and chalcone motifs, to target PUD, particularly focusing on *H. pylori* infection. Employing various spectroscopic techniques such as FT-IR, NMR and elemental analysis, we aim to elucidate the chemical structure and confirm the purity of the synthesized compounds. Density Functional Theory (DFT) studies will unravel the reactivity profiles, shedding light on the molecular intricacies governing their behavior. Molecular docking studies onto *H. pylori* receptors will provide valuable insights into the binding affinity and potential therapeutic efficacy of the novel compounds, steering us toward innovative solutions for combating PUD.

2. Results and discussion

2.1. Chemistry

In pursuit of expanding the repertoire of biologically active compounds, our focus has centered on the benzothiazole and pyrazole heterocycles [27,28]. Drawing inspiration from their inherent biological activities, we embarked on a series of endeavors to functionalize these molecules. A meticulously designed synthetic pathway, as illustrated in Scheme 1, has facilitated the straightforward and efficient synthesis of the target compounds **4a-c**. The structures elucidation confirmed through IR, ^{1}H NMR, ^{13}C NMR and elemental analysis. Cyclocondensation of 2-hydrazinobenzothiazole **1** with ethyl acetoacetate in ethanol gives 5-pyrazolones **2** which undergoes acetylation by Jensen's procedure using acetyl chloride in dioxane as a solvent in the presence of calcium hydroxide to form 4-acetyl-5-pyrazolone derivative **3** in a good yield. The chalcone derivatives **4a-c** were prepared as Claisen's Schimidt reaction of compound **3** with different aromatic aldehyde by using sodium hydroxide in ethanol at 0 °C, Scheme 1.

The FT-IR spectra of chalcones **4a-c** showed two strong absorption bands ranging 1710–1705 and 1696–1690 cm^{-1} attributed to stretching vibration of carbonyl of pyrazolone ring and keto group, respectively. The medium absorption band at 1633–1619 cm^{-1} ascribed to the vibration of imino (C═N) group [29,30]. Additionally, the aromatic (=C–H) and aliphatic (-C-H) stretching vibrations appeared as weak absorption bands in range 3072–3037 and 2960–2918 cm^{-1}, respectively.

The ^{1}H NMR spectral data of **4a-c** exhibited two singlets at range δ 3.76–3.30 and 1.89–1.55 ppm due to the presence of pyrazolone CH and methyl group at position **3**, respectively. Furthermore, the olefinic protons (CH═CH) appeared as two doublet signals at δ 7.48–7.14 and 6.89–6.70 ppm. Additionally, ^{1}H NMR spectra showed multiplets at δ 8.29–6.72 ppm that ascribed the aromatic protons of phenyl and benzothiazole rings.

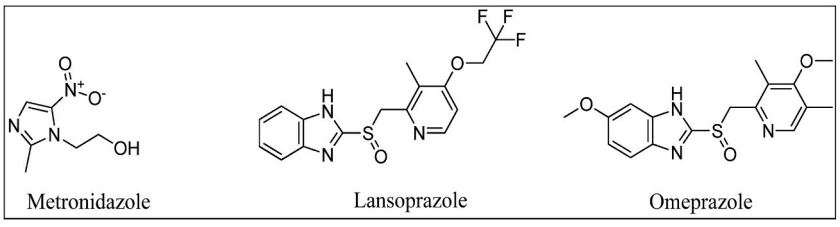

Fig. 1. Commercial drugs for treatments of *H. pylori* infection.

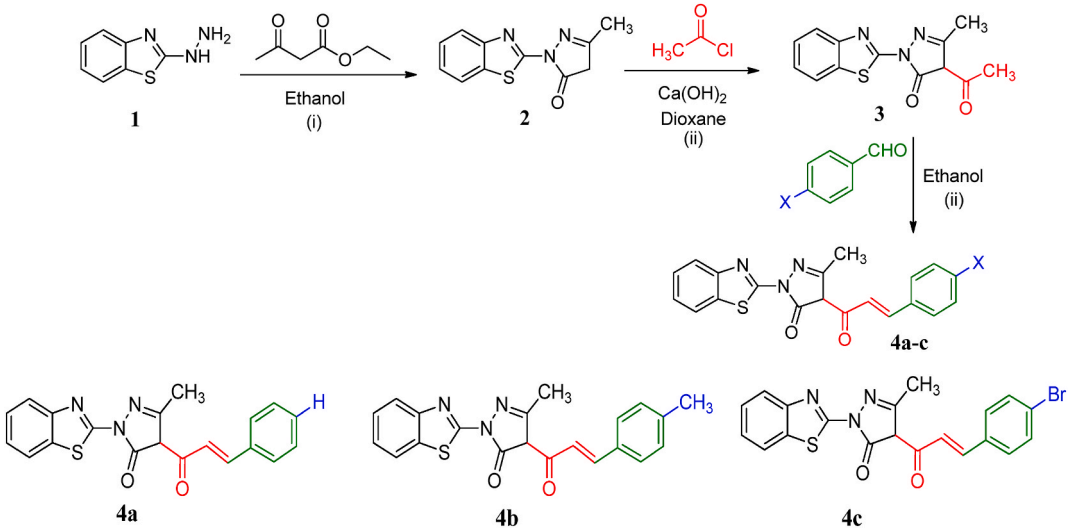

Scheme 1. Synthesis of chalcones **4a-c**
Reagents and conditions: (i) Ethanol, reflux 1 h; yield (83.05 %). (ii) Dioxane and calcium hydroxide, reflux 0.5 h, HCl (2 N); yield (75.17 %). (iii) Ethanol and NaOH, stirring 0.5 h; yield (65.14–69.88%).

2.2. DFT computional studies

2.2.1. Geometrical and thermal parameters

Chalcones are versatile compounds that can be structurally modified to tune their characteristics for various applications specially their biological activity. Density functional theory (DFT) calculations were performed on newly synthesized chalcone derivatives **4a-c** to determine key thermal and electronic properties. Furthermore, the calculated quantum chemical parameters and optimized geometries provide a foundation to understand the structure-activity relationships that may govern the biological activity of chalcone derivatives **4a-c**. DFT methods allow efficient prediction of molecular properties based on the electron density distribution. B3LYP hybrid functional with the 6-311G basis set was selected, as it generally provides good accuracy for organic systems. The absence of an imaginary frequency in the optimized geometrical structures not only underscores their stability but also serves as a visual testament, as illustrated in Fig. 2. The optimized geometries, thermal parameters, polarizabilities, and dipole moments were computed to gain insight into how the substituents impact the properties, Table 1.

The electron-donating and -withdrawing substituents can modulate key molecular properties like binding affinity, cell permeability, and enzyme inhibition profiles that dictate therapeutic potential [31,32]. The DFT results reveal how the electron-donating (*p*-tolyl, **4b**) and electron-withdrawing (*p*-bromophenyl, **4c**) moieties modulate the chalcone derivatives. The *p*-tolyl derivative **4b** has the highest thermal stability in terms of enthalpy, Gibbs free energy, and entropy that could enhance its potency or bioavailability compared to **4a** and **4c**. This can be attributed to greater delocalization of π electrons provided by the methyl group. In contrast, the *p*-bromophenyl compound **4c** possesses the lowest thermal character. The electron-withdrawing bromine likely restricts resonance. Polarizability followed the order **4c** > **4b** > **4a**, indicating **4c** is the most polarizable. The dipole moments show a trend **4b** > **4a** > **4c**, which may be due to the increasing of donating ability.

2.2.2. Frontier molecular orbitals

The highest occupied molecular orbital (HOMO) and lowest unoccupied molecular orbital (LUMO) of a molecule, known as frontier molecular orbitals (FMOs), play a key role in determining its bioactivity. The HOMO, containing the highest energy electrons, acts as an electron donor while the LUMO can accept electrons into its lowest energy unfilled orbital. The energies of HOMO and LUMO

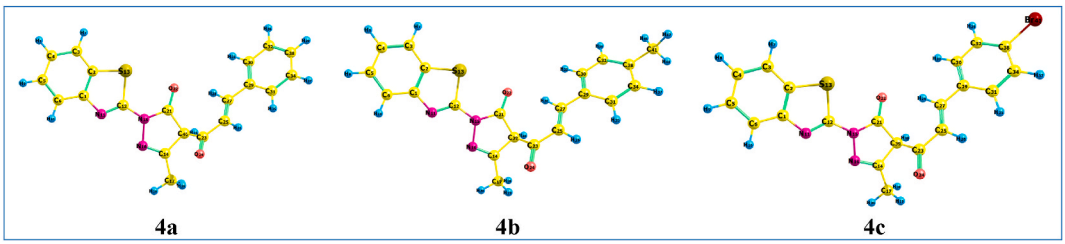

Fig. 2. Optimized structures of chalcones **4a-c**.

Table 1
Calculated thermal parameters, dipole moment and polarizability of chalcone derivatives **4a-c**.

Compound	ZPE (Kcal/Mol)	Thermal energy (Kcal/Mol)	Enthalpy (Kcal/Mol)	Gibbs free energy (Kcal/Mol)	Entropy (Cal mol.k)	Polarizability (α) $Bohr^3$	Dipole moment (D)
4a	195.402	208.818	209.411	162.172	158.441	257.856	4.595
4b	212.641	227.2573	227.850	177.6446	168.391	275.193	5.312
4c	189.300	203.597	204.189	154.164	167.788	279.884	3.344

orbitals indicate the chemical reactivity of a molecule, with small HOMO-LUMO energy gaps generally corresponding to high reactivity. Additionally, the spatial distribution of FMOs influences the binding interactions of a molecule with biological receptors [33,34]. The present study analyzes the FMOs of three compounds **4a-c** to determine how their electronic properties may modulate bioactivity, Table 2. The HOMO electron densities are distributed over the benzothiazolyl rings, while the LUMO electron densities extend onto the α,β-unsaturated carbonyl group, Fig. 3. This indicates that the benzothiazolyl rings act as the electron donors and the olefinic unit acts as the electron acceptor. Among the three compounds 4a-**4c,** 4**c** has the lowest energy HOMO at −6.1382 eV while 4**a** has the highest energy HOMO at −6.0854 eV. For the LUMO orbital energies, 4**c** also has the lowest energy at −2.5388 eV while **4b** has the highest LUMO energy at −2.3148 eV. Molecules with large energy gaps are known as hard molecules and possess higher thermal stabilities [35,36]. The decreasing order of HOMO-LUMO energy gaps (**ΔE)** is: 4**b** > 4**a** > 4**c**. The smaller **ΔE** in 4**c** suggests it likely has higher chemical reactivity compared to **3a** and 4a.

2.2.3. Chemical reactivity descriptors

The global chemical reactivity descriptors calculated using DFT provide valuable insights into the structure-stability-reactivity relationships of the new compounds **4a-c**. The energies of HOMO and LUMO are key quantum chemical parameters that determine molecular reactivity and are utilized to derive important descriptors like electron affinity (EA), ionization potential (IP), chemical potential (μ), absolute electronegativity (χ), softness (σ), hardness (η), and electrophilicity (ω). Among these, high hardness (η) indicates low binding potential whereas high softness (σ) suggests strong binding interactions [37]. Additionally, low electronegativity (χ) values typically correspond to enhanced receptor binding affinity. The chemical potential (μ) reveals the electron donating/-accepting aptitude, with higher values pointing to improved binding interactions.

An analysis of the parameters in Table 2 indicates that compound 4**c** possesses the highest electronegativity (χ) value of 4.3385 eV, making it the most electron withdrawing of the series. Additionally, 4**c** exhibits the highest chemical potential (μ) at −4.3385 eV, suggesting its enhanced ability to accept electrons. In contrast, 4**a** with the highest energy HOMO (−6.0854 eV) and highest ionization potential (IP) of 6.0854 eV is expected to readily donate electrons. Regarding stability, 4**b** has the highest hardness (η) of 1.8687 eV among the compounds, implying it is the most inert, while **3c** with a hardness of 1.7998 eV is anticipated to be the most reactive. Moreover, the softness (σ) order of 4**c** > 4**a** > 4**b** agrees with this relative reactivity trend.

2.2.4. Molecular electrostatic potential (MEP)

The molecular electrostatic potential (MEP) maps provide critical insights into the distribution of electron density and electrostatic potential in compounds **4a-c**, validating their predicted reactivity. As depicted in Fig. 4, the MEP maps were generated by DFT calculations. In these maps, the red clouds represent high electron density regions which act as nucleophiles. The blue clouds highlight areas of low electron density that correspond to electropositive sites and are prone to electrophilic addition reactions. For compounds **4a-c**, the red clouds are localized on the electronegative heteroatoms (N, O and S). In contrast, the blue regions spread out over the electropositive phenyl rings. The complementary electrostatic potentials can facilitate molecular recognition processes like drug-receptor binding by enabling attractive interactions between electronegative and electropositive sites.

Table 2
Calculated Chemical descriptor parameters of chalcones **4a-c**.

Parameter	4a	4b	4c
E_{HOMO} (eV)	−6.0854	−6.0522	−6.1382
E_{LUMO} (eV)	−2.3951	−2.3148	−2.5388
ΔE (eV)	3.6903	3.7374	3.5994
IP (eV)	6.0854	6.0522	6.1382
EA (eV)	2.3951	2.3148	2.5388
χ (eV)	4.2402	4.1835	4.3385
μ (eV)	−4.2402	−4.1835	−4.3385
η (eV)	1.8452	1.8687	1.7998
σ (eV^{-1})	0.5420	0.5351	0.5556
ω (eV)	4.8721	4.6829	5.2293

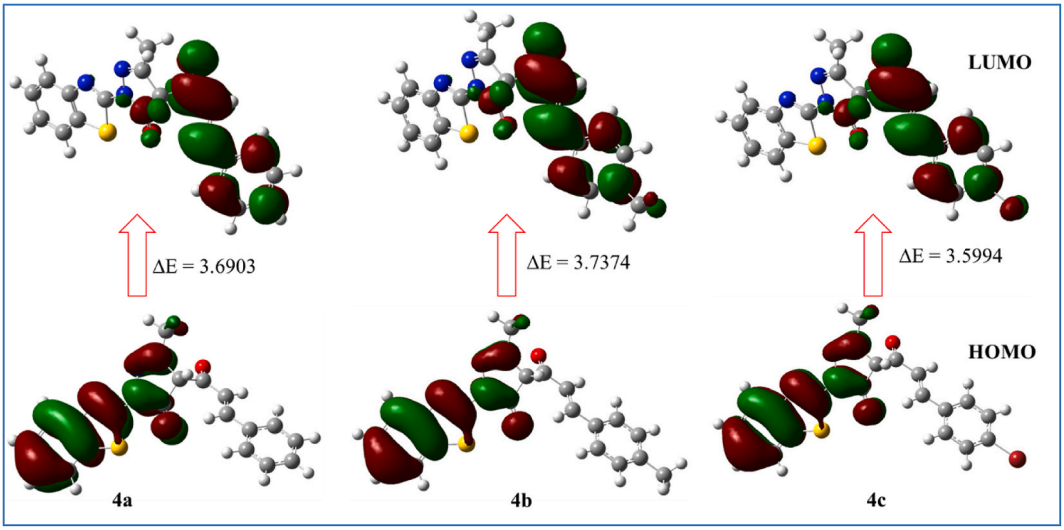

Fig. 3. The estimated ground state plots of Frontier molecular orbitals (FMOs) for chalcones **4a-c**.

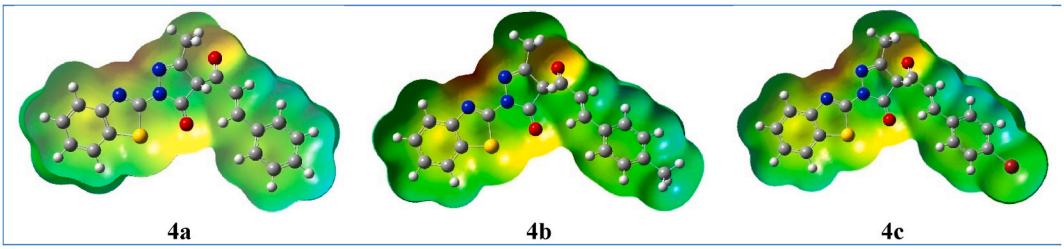

Fig. 4. Molecular electrostatic potentials (MEP) of chalcone **4a-c**.

2.3. Molecular docking

Molecular docking has become an invaluable tool in computer-aided drug design, allowing prediction of ligand binding modes and affinity for target proteins prior to in vitro testing. By modeling the interactions between small molecules and biological receptors at the molecular level, docking provides critical insights that can accelerate and streamline experimental screening efforts [38,39]. By leveraging *in silico* predictions pre-experimentally, molecular docking improves the efficiency of early-phase drug discovery, reducing associated costs and resources as well as guiding ongoing discovery to promising chemical scaffolds. Molecular docking studies were conducted to investigate the binding interactions between ligands **4a-c** and the urease protein (PDB: 2QV3) [40] from *H. pylori,* an important target for anti-ulcer drug discovery, using MOE (2015). The ligands **4a-c** were docked into the active site of the urease enzyme to predict their binding modes and affinity.

The docking results showed that ligands **4a-c** bind to the active site amino acids of urease of *Helicobacter pylori*, with docking scores (S) ranging from −5.3862 to −5.7367 kcal/mol, Table 3, with improved predicted binding affinities versus the reference ligand lansoprazole. The key amino acids involved in interactions with the ligands are ASN666, SER714, and ASN810. The interactions identified include hydrogen bond donor and hydrophobic pi-hydrogen bond between the ligand chemical groups and active site residues.

Table 3
Docking results of **4a-c** docked into urease protein (PDB: 2QV3) from *Helicobacter pylori*.

Ligand	S (kcal/mol)	Type of interaction	Ligand - Receptor	Distance (A^o)
4a	−5.3862	H-donor	S41 - ASN 666	3.55
		pi-H	5-ring - ASN 810	4.18
4b	−5.5621	H-donor	S44 - ASN 666	4.01
		pi-H	5-ring - ASN 810	4.19
4c	−5.7368	pi-H	6-ring - SER 714	3.46
		pi-H	5-ring - ASN 810	4.34
Lansoprazole	−5.3629	pi- H	6-ring - ASN 711	4.27

Specifically, ligand **4a** displayed a hydrogen bond interaction between the S41 atom and ASN666 residue at a distance of 3.55 Å, Figs. 5–6. It also formed a pi-hydrogen bond between its 5-membered ring and ASN810 at 4.18 Å distance. Similarly, ligands **4b** and **4c** showed hydrogen bond donor and pi-hydrogen bonds with distances ranging from 3.46 to 4.34 Å involving ASN666, SER714 and ASN810 amino acids. These *in silico* results provide strong preliminary evidence that the novel ligands **4a-c** could effectively inhibit urease enzymatic activity and may represent promising new anti-ulcer agents.

3. Conclusions

This study reports the successful synthesis and structural characterization of a novel series of chalcone derivatives bearing benzothiazole and pyrazoline moieties as potential anti-ulcer agents targeting *H. pylori* infection. Spectroscopic techniques were used to confirm the structures of chalcones **4a-c** such as FT-IR, NMR and elemental analysis. The DFT-predicted reactivity agreed well with the structure-activity relationships. The *p*-tolyl derivative **4b** exhibiting the largest HOMO-LUMO gap of 3.7374 eV, indicating its high stability. In contrast, the *p*-bromophenyl compound **4c** with the lowest gap of 3.5994 eV suggesting increased reactivity. Molecular docking predicted promising binding interactions with the *H. pylori* urease enzyme, as evidenced by favorable docking scores (−5.3862 to −5.7367 kcal/mol) and key hydrogen bond/hydrophobic contacts with active site residues. This combined experimental and computational study paves the pathway for further optimization of this novel series of chalcones to treat ulcers associated with *H. pylori* infection.

4. Materials and methods

4.1. Measurements

Melting point determinations were carried out using a precision Koffler block, and all reported values are uncorrected. The molecular structures and functional groups were elucidated through Fourier Transform Infrared (FT-IR) spectroscopy, performed on a Perkin Elmer-USA Spectrometer, Alexandria University, Alexandria, Egypt. FT-IR spectra were recorded at room temperature, covering a broad wave number range from 4000 to 400 cm^{-1}. NMR spectra were acquired on a high-field JEOL JNM ECA 400 MHz instrument, Alexandria University, Alexandria, Egypt. Tetramethylsilane was used as an internal standard, and the solvent of choice was DMSO-d_6, maintaining the samples at a constant temperature of 25 °C. The resulting chemical shifts (δ) were expressed in parts per million (ppm).

4.1.1. Synthesis of 2-(benzo[d]thiazol-2-yl)-5-methyl-2,4-dihydro-3H-pyrazol-3-one 2

A mixture of 2-hydrazinobenzothiazole **1** (0.005 mol, 0.825 gm) **1** and ethyl acetoacetate (0.005 mol, 0.656 gm) in 20 mL absolute ethanol was refluxed for 1 h. The completion of the reaction was indicated by TLC. The reaction mixture was cooled and the solid obtained was filtered, dried and recrystallized from ethanol to give yellow crystal. Yield: 83.05 %, m.p. 150–152 °C. FT-IR (KBr): ν

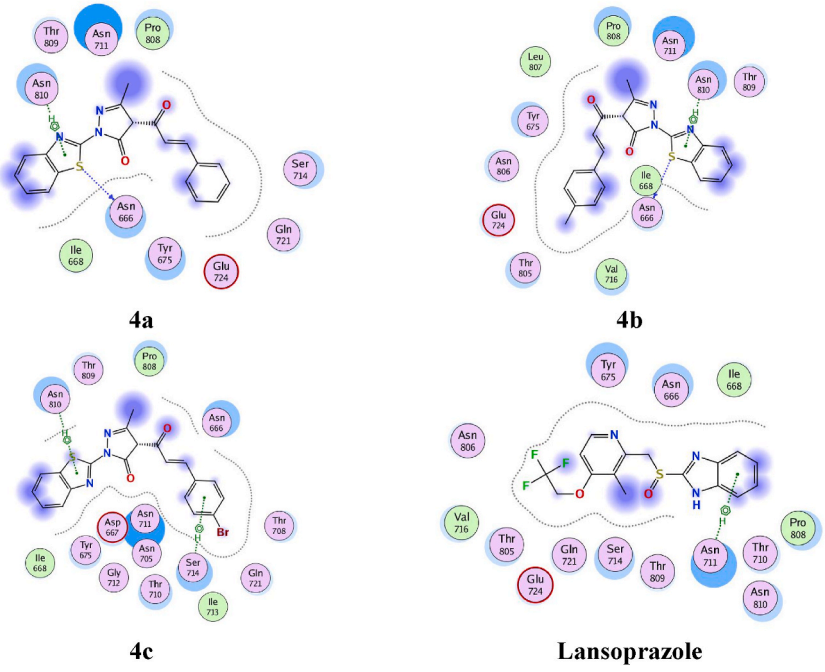

Fig. 5. 2D binding modes of **4a-c** onto urease protein (PDB: 2QV3) from *Helicobacter pylori*.

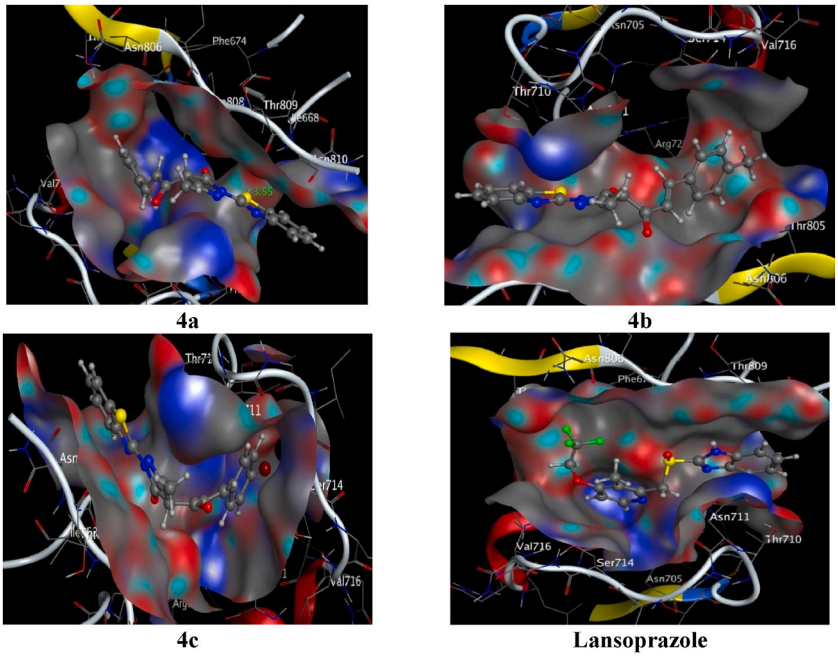

Fig. 6. 3D binding modes of **4a-c** in urease protein (PDB: 2QV3) from *Helicobacter*.

3078 (Sp^2 = CH), 2964 (Sp^3 –CH), 1737 (C═O), 1649 (C═N) and 1614 (C═C) cm^{-1}. ^{1}H NMR (400 MHz, DMSO-*d*6): δ 7.60 (d, 1H, Ar-H), 7.39 (d, 1H, Ar-H), 7.31 (t, 2H, Ar-H), 3.44 (s, 2H, CH_2) and 1.94 (s, 3H, CH_3) ppm. ^{13}C NMR (101 MHz, DMSO-*d*6): δ 174.5, 170.0, 153.2, 152.9, 130.8, 125.3, 124.5, 121.8, 118.3, 42.5 and 16.7 ppm. $C_{11}H_9N_3OS$ requires C, 57.13; H, 3.92; N, 18.17 %. Found: C, 57.04; H, 3.89; N, 18.23.

4.1.2. Synthesis of 4-acetyl-2-(benzo[d]thiazol-2-yl)-5-methyl-2,4-dihydro-3H-pyrazol-3-one 3

15.0 gm of 2-(benzo[*d*]thiazol-2-yl)-5-methyl-2,4-dihydro-3*H*-pyrazol-3-one **2** was dissolved in 80 mL dioxane and heated under reflux system. 12 gm of calcium hydroxide was added followed by dropwise addition of 7.5 mL acetyl chloride with 5 min. The reaction mixture become a thick paste after few minutes. The mixture was continue heating for 30 min. The calcium complex formed was decomposed by pouring the mixture into hydrochloric acid (2 mL, 2 N) forming solid product. The product was filtered, dried and recrystallized from ethanol to form yellow crystals. Yield: 75.17 %. m.p. 161–163 °C. FT-IR (KBr): ν 3063 (Sp^2 = CH), 2956 (Sp^3 –CH), 1748 (C═O), 1727 (C═O), 1637 (C═N) and 1602 (C═C) cm^{-1}. ^{1}H NMR (400 MHz, DMSO-*d*6): δ 7.81 (d, 2H, Ar-H), 7.79 (t, 2H, Ar-H), 3.73 (s, 1H, CH), 2.93 (s, 3H, CH_3) and 1.95 (s, 3H, CH_3) ppm. ^{13}C NMR (101 MHz, DMSO-*d*6): δ 196.2, 174.6, 169.1, 155.6, 153.4, 130.7, 125.3, 124.3, 121.5, 118.8, 60.2, 27.8 and 21.9 ppm. $C_{13}H_{11}N_3O_2S$ requires C, 57.13; H, 4.06; N, 15.37 %. Found: C, 57.09; H, 4.12; N, 15.25.

4.1.3. General procedure for synthesis investigated compound 4a-c

To a mixture of compound **3** (1.0 gm, 3.6 mmol) in 20 mL ethanol and NaOH (0.15 gm, 3.75 mmol) in 5 mL H_2O at 0 °C was gradually added aromatic aldehyde (benzaldehyde, *p*-tolaldehyde, *p*-bromobenzaldehyde) (3.6 mmol). The mixture was stirred for 3 h, after which the precipitate was collected by suction filtration and washed repeatedly with cold water. The residue was recrystallized from ethanol.

4.1.4. (E)-2-(benzo[d]thiazol-2-yl)-4-cinnamoyl-5-methyl-2,4-dihydro-3H-pyrazol-3-one 4a

Brown crystal, yield: 65.14 %. m.p. 89–91 °C. FT-IR (KBr): ν 3059 (Sp^2 = CH), 2918 (Sp^3 –CH), 1705 (C═O), 1695 (C═O), 1633 (C═N) and 1616 (C═C) cm^{-1}. ^{1}H NMR (400 MHz, DMSO-*d*6): δ 8.28 (d, 2H, Ar-H), 7.96-7.40 (m, 7H, Ar-H), 7.23 (d, 1H, =CH-Ar), 6.79 (d, 1H, –CH =), 3.76 (s, 1H, CH) and 1.56 (s, 3H, CH_3) ppm. ^{13}C NMR (101 MHz, DMSO-*d*6): δ 193.5, 174.1, 169.7, 154.4, 152.1, 142.8, 135.2, 130.5, 128.6, 128.5, 127.9, 125.1, 124.5, 121.8, 117.2, 58.0, and 21.7 ppm. $C_{20}H_{15}N_3O_2S$ requires C, 66.46; H, 4.18; N, 11.63 %. Found: C, 66.52; H, 4.13; N, 11.52.

4.1.5. (E)-2-(benzo[d]thiazol-2-yl)-4-(3-(p-tolyl)acryloyl)-5-methyl-2,4-dihydro-3H-pyrazol-3-one 4b

Orange crystal, yield: 69.88 %, m.p. 84–86 °C. FT-IR (KBr): ν 3072 (Sp^2 = CH), 2960 (Sp^3 –CH), 1710 (C═O), 1690 (C═O), 1633 (C═N) and 1600 (C═C) cm^{-1}. ^{1}H NMR (400 MHz, DMSO-*d*6): δ 7.84-7.65 (m, 4H, Ar-H), 7.41 (d, 2H, ArH), 7.14 (d, 1H, =CH-Ar), 6.80-6.72 (m, 2H, Ar-H), 6.70 (d, 1H, –CH =), 3.69 (s, 1H, CH), 2.18 (s, 3H, CH_3) and 1.55 (s, 3H, CH_3) ppm. ^{13}C NMR (101 MHz, DMSO-*d*6): δ 192.1, 170.5, 167.3, 154.2, 153.0, 140.5, 136.1, 132.6, 131.2, 128.7, 128.5, 126.7, 125.2, 124.3, 121.7, 118.0, 57.9, 21.9

and 21.7 ppm. $C_{21}H_{17}N_3O_2S$ requires C, 67.18; H, 4.56; N, 11.19 %. Found: C, 67.25; H, 4.44; N, 11.25.

4.1.6. (E)-2-(benzo[d]thiazol-2-yl)-4-(3-(4-bromophenyl)acryloyl)-5-methyl-2,4-dihydro-3H-pyrazol-3-one 4c

Orange crystal, yield: 67 %. m.p. 91–93 °C. FT-IR (KBr): ν 3037 (Sp^2 = CH), 2960 (Sp^3 –CH), 1710 (C═O), 1696 (C═O), 1619 (C═N) and 1599 (C═C) cm^{-1}. ^{1}H NMR (400 MHz, DMSO-*d*6): δ 8.29 (d, 2H, Ar-H), 7.69–7.78 (m, 2H, Ar-H), 7.61 (d, 2H, Ar-H), 7.50 (d, 2H, Ar-H), 7.48 (d, 1H, =CH-Ar), 6.76 (d, 1H, –CH =), 3.30 (s, 1H, CH) and 1.89 (s, 3H, CH_3) ppm. ^{13}C NMR (101 MHz, DMSO-*d*6): δ 191.2, 171.0, 167.4, 155.1, 150.9, 140.5, 133.5, 129.8, 129.4, 128.1, 127.6, 125.7, 123.9, 122.1, 121.5, 117.2, 58.4, and 20.9 ppm. $C_{20}H_{14}BrN_3O_2S$ requires C, 54.56; H, 3.20; N, 9.54 %. Found: C, 54.62; H, 3.15; N, 9.59.

4.2. Quantum chemical calculations

We utilized Gaussian 09 software suite for all quantum mechanical calculations. The calculations were performed employing the popular B3LYP functional, renowned for its accuracy in predicting molecular properties [41]. To ensure reliable results, a 6-31G(d,p) basis set was employed. This computational framework served for elucidating the electronic structure and reactivity profiles of the synthesized compounds.

4.3. Docking program

In our study to understand the binding interactions between our newly synthesized compounds **4a-c** and the urease protein from *H. pylori*, molecular docking simulations were meticulously executed. The crystal structure of the urease protein (PDB ID: 2QV3) [40] served as the receptor, obtained from the Protein Data Bank (www.rcsb.org). To ensure the reliability of the simulations, a series of preparatory steps were undertaken. The structures of the compounds were initially subjected to a conformational search using the Monte Carlo method with the MMFF94 molecular mechanics model. This step aimed to optimize the energy and geometry of the ligands before the docking process. The Molecular Operating Environment (MOE) Software version 2015 was instrumental in both preparing the input files and analyzing the results. The preparation of the protein input file involved the removal of water molecules, ligands, and ions from the PDB file, ensuring a focused analysis of the compound-urease interactions. The identification of active sites within the urease protein was performed using the 'Site Finder' feature in MOE 2015, enhancing the precision of our docking simulations. Multiple docking simulations were carried out, employing various fitting protocols to observe the diverse molecular interactions and assess free binding energies comprehensively. The compound-urease complexes generated through these simulations were systematically ranked based on energy scores, taking into account their binding conformations.

Data availability statement

Data included in article/supplementary material/referenced in article.

Funding

This research was funded by Princess Nourah bint Abdulrahman University Researchers Supporting Project number (PNURSP2024R403), Princess Nourah bint Abdulrahman University, Riyadh, Saudi Arabia.

CRediT authorship contribution statement

Najla A. Alshaye: Writing – original draft, Software, Formal analysis, Data curation. **Nuha Salamah Alharbi:** Writing – original draft, Resources, Formal analysis. **Mohamed A. El-Atawy:** Writing – review & editing, Writing – original draft, Resources, Investigation, Data curation. **Reham O. El-Zawawy:** Writing – original draft, Software, Resources, Methodology, Data curation. **Ezzat A. Hamed:** Writing – review & editing, Supervision. **Mohammed Elhag:** Writing – original draft, Methodology, Investigation. **Hoda A. Ahmed:** Writing – original draft, Software, Investigation. **Alaa Z. Omar:** Writing – review & editing, Writing – original draft, Software, Methodology, Formal analysis, Data curation.

Declaration of competing interest

The authors declare that they have no known competing financial interests or personal relationships that could have appeared to influence the work reported in this paper.

Acknowledgements

The authors extend their sincere appreciation to Princess Nourah bint Abdulrahman University Researchers Supporting Project number (PNURSP2024R403), Princess Nourah bint Abdulrahman University, Riyadh, Saudi Arabia.

Appendix A. Supplementary data

Supplementary data to this article can be found online at https://doi.org/10.1016/j.heliyon.2024.e34540.

References

[1] P. Ravisankar, O. Koushik, A. Reddy, A. Kumar, P. Pragna, A detailed analysis on acidity and ulcers in esophagus, gastric and duodenal ulcers and management, J. Dent. Med. Sci. 15 (2016) 94–114.
[2] A. Ali, A. Mohamed, Y. Mohamed, S. Keleşoğlu, Clinical presentation and surgical management of perforated peptic ulcer in a tertiary hospital in Mogadishu, Somalia: a 5-year retrospective study, World J. Emerg. Surg. 17 (2022) 1–8.
[3] D. Sierra, M. Wood, S. Kolli, L. Felipez, Pediatric gastritis, gastropathy, and peptic ulcer disease, Pediatr. Rev. 39 (2018) 542–549.
[4] D. Bhowmik, T. Chiranjib, K. Pankaj, Recent trends of treatment and medication peptic ulcerative disorder, Int. J. Pharm. Tech. Res. 2 (2010) 970–980.
[5] M. Prasad, J. Tokar, Acute gastrointestinal bleeding, Ann. Intern. Med. 159 (2013) 1–9.
[6] J. Khatoon, R. Rai, K. Prasad, Role of Helicobacter pylori in gastric cancer: Updates, World J. Gastrointest. Oncol. 8 (2016) 147–158.
[7] S. Zhang, Y. Shen, H. Liu, D. Zhu, J. Fang, H. Pan, W. Liu, Inflammatory microenvironment in gastric premalignant lesions: implication and application, Front. Immunol. 14 (2023) 45–54.
[8] C.-Y. Kao, B.-S. Sheu, J.-J. Wu, Helicobacter pylori infection: an overview of bacterial virulence factors and pathogenesis, Biomed. J. 39 (2016) 14–23.
[9] J. Baj, A. Forma, M. Sitarz, P. Portincasa, G. Garruti, D. Krasowska, R. Maciejewski, Helicobacter pylori virulence factors—mechanisms of bacterial pathogenicity in the gastric microenvironment, Cells 10 (2020) 27–39.
[10] Y. Liu, H. Tang, Z. Lin, P. Xu, Mechanisms of acid tolerance in bacteria and prospects in biotechnology and bioremediation, Biotechnol. Adv. 33 (2015) 1484–1492.
[11] S. Mazumder, S. Bindu, R. De, S. Debsharma, S. Pramanik, U. Bandyopadhyay, Emerging role of mitochondrial DAMPs, aberrant mitochondrial dynamics and anomalous mitophagy in gut mucosal pathogenesis, Life Sci. (2022) 120753–120762.
[12] S. Ansari, Y. Yamaoka, Helicobacter pylori virulence factors exploiting gastric colonization and its pathogenicity, Toxins 11 (2019) 677–686.
[13] N. Hage, T. Howard, C. Phillips, C. Brassington, R. Overman, J. Debreczeni, P. Gellert, S. Stolnik, G. Winkler, F. Falcone, Structural basis of Lewisb antigen binding by the Helicobacter pylori adhesin BabA, Sci. Adv. 1 (2015) e1500315.
[14] P. Manikanta, Mounesh, R.R. Nikam, S. Sandeep, B.M. Nagaraja, Development of novel microsphere structured – calcium tungstate as efficacious electrocatalyst for the detection of antibiotic drug nitrofurantoin, J. Mater. Chem. 11 (2023) 11600–11611, https://doi.org/10.1039/D3TB02087H.
[15] B. Manjunatha, Y.D. Bodke, Mounesh, O. Nagaraja, P.V. Navaneethgowda, Coumarin-pyridone conjugate as a fluorescent tag for LFPs visualization and electrochemical sensor for nitrite detection, New J. Chem. 46 (2022) 5393–5404, https://doi.org/10.1039/D1NJ04751E.
[16] B. Manjunatha, Y.D. Bodke, S.A. Bhat, Coumarin-based composite material for the latent fingerprint visualization and electrochemical sensing of hydrogen peroxide, RSC Sustain 2 (2024) 475–482.
[17] C. Kharbanda, M.S. Alam, H. Hamid, K. Javed, S. Bano, A. Dhulap, Y. Ali, S. Nazreen, S. Haider, Synthesis and evaluation of pyrazolines bearing benzothiazole as anti-inflammatory agents, Bioorg. Med. Chem. 22 (2014) 5804–5812.
[18] K. Gupta, A.K. Sirbaiya, V. Kumar, M.A. Rahman, Current perspective of synthesis of medicinally relevant benzothiazole based molecules: potential for antimicrobial and anti-inflammatory activities, Mini-Rev. Med. Chem. 22 (2022) 1895–1935.
[19] A.Z. Omar, T.M. Mosa, S.K. El-sadany, E.A. Hamed, M. El-atawy, Novel piperazine based compounds as potential inhibitors for SARS-CoV-2 Protease Enzyme: synthesis and molecular docking study, J. Mol. Struct. 1245 (2021) 131020, https://doi.org/10.1016/j.molstruc.2021.131020.
[20] H.E. Abdelwahab, H.Z. Ibrahim, A.Z. Omar, Design, synthesis, DFT, molecular docking, and biological evalution of pyrazole derivatives as potent acetyl cholinestrease inhibitors, J. Mol. Struct. 1271 (2023) 134137, https://doi.org/10.1016/j.molstruc.2022.134137.
[21] A. Gupta, S. Shetty, S. Mutalik, K. Nandakumar, E.M. Mathew, A. Jha, B. Mishra, S. Rajpurohit, G. Ravi, M. Saha, Treatment of H. pylori infection and gastric ulcer: need for novel Pharmaceutical formulation, Heliyon 9 (2023) e20406, 145-157.
[22] A. Husain, S.A. Khan, F. Iram, M.A. Iqbal, M. Asif, Insights into the chemistry and therapeutic potential of furanones: a versatile pharmacophore, Eur. J. Med. Chem. 171 (2019) 66–92.
[23] D. Becerra, R. Abonia, J.-C. Castillo, Recent applications of the multicomponent synthesis for bioactive pyrazole derivatives, Molecules 27 (2022) 4723–4736.
[24] S.-R. Li, Y.-M. Tan, L. Zhang, C.-H. Zhou, Comprehensive insights into medicinal research on imidazole-based supramolecular complexes, Pharm. Times 15 (2023) 1348–1360.
[25] G. Rajendran, D. Bhanu, B. Aruchamy, P. Ramani, N. Pandurangan, K.N. Bobba, E.J. Oh, H.Y. Chung, P. Gangadaran, B.-C. Ahn, Chalcone: a promising bioactive scaffold in medicinal chemistry, Pharm. Times 15 (2022) 1250.
[26] R.M. Borik, Novel chalcone derivatives containing pyridone and thiazole moieties: design, synthesis, molecular docking, antibacterial, and antioxidant activities, Curr. Org. Chem. 27 (2023) 1960–1977.
[27] S. Bondock, W. Fadaly, M.A. Metwally, Enaminonitrile in heterocyclic synthesis: synthesis and antimicrobial evaluation of some new pyrazole, isoxazole and pyrimidine derivatives incorporating a benzothiazole moiety, Eur. J. Med. Chem. 44 (2009) 4813–4818.
[28] V. Padalkar, B. Borse, V. Gupta, K. Phatangare, V. Patil, N. Sekar, Synthesis and antimicrobial activities of novel 2-[substituted-1*H*-pyrazol-4-yl] benzothiazoles, benzoxazoles, and benzimidazoles, J. Heterocycl. Chem. 53 (2016) 1347–1355, 1364.
[29] A. Omar, M. Mohamed, E. Hamed, M. El-atawy, Characterization, DFT calculations and dyeing performance on polyester fabrics of some azo disperse dyes containing pyrazole ring, J. Saudi Chem. Soc. 27 (2023) 101594, https://doi.org/10.1016/j.jscs.2022.101594.
[30] M. El-Atawy, A. Omar, M. Alazmi, M. Alsubaie, E. Hamed, H. Ahmed, Synthesis and characterization of new imine liquid crystals based on terminal perfluoroalkyl group, Heliyon 9 (2023) e14871, https://doi.org/10.1016/j.heliyon.2023.e14871.
[31] R. Ahmad, A. Alam, M. Khan, T. Ali, A.A. Elhenawy, M. Ahmad, Antioxidant activity, molecular docking and quantum studies of new bis-schiff bases based on benzyl phenyl ketone moiety, ChemistrySelect 8 (2023) e202302338.
[32] V. Sharma, M. Gupta, P. Kumar, A. Sharma, A comprehensive review on fused heterocyclic as DNA intercalators: promising anticancer agents, Curr. Pharm. Des. 27 (2021) 15–42.
[33] R. El-Zawawy, A. Ali, M. Masoud, A. Omar, Synthesis, structural, DFT, and antimicrobial studies of some cefprozil complexes, Russ. J. Gen. Chem. 93 (2023) 2960–2972.
[34] M. El-Atawy, M. Alsubaie, M. Alazmi, E. Hamed, D. Hanna, H. Ahmed, A. Omar, Synthesis, characterization, and anticancer activity of new N,N-diarylthiourea derivative against breast cancer cells, Molecules 28 (2023) 6420–6429.
[35] A. Omar, M. Mahmoud, S. El-Sadany, E. Hamed, M. El-atawy, A combined experimental and DFT investigation of mono azo thiobarbituric acid based chalcone disperse dyes, Dyes Pigments 185 (2021) 108887, https://doi.org/10.1016/j.dyepig.2020.108887.
[36] A. Omar, M. El-Rahman, S. El-Sadany, E. Hamed, M. El-Atawy, Synthesis of novel bisazo disperse dyes: spectroscopic characterization, DFT study and dyeing of polyester, Dyes Pigments 196 (2021) 109831, https://doi.org/10.1016/j.dyepig.2021.109831.
[37] A. Omar, M. El-Atawy, M. Alsubaie, M. Alazmi, H. Ahmed, E. Hamed, Synthesis and computational investigations of new thioether/azomethine liquid crystal derivatives, Crystals 13 (2023) 378–386.
[38] X.-Y. Meng, H.-X. Zhang, M. Mezei, M. Cui, Molecular docking: a powerful approach for structure-based drug discovery, Curr. Comput. Aided Drug Des. 7 (2011) 146–157.

[39] M. El-Atawy, N. Alshaye, N. Elrubi, E. Hamed, A. Omar, Pyrimidines-based heterocyclic compounds: synthesis, cytoxicity evaluation and molecular docking, Molecules 27 (2022) 4912–4924.
[40] K.A. Gangwer, D.J. Mushrush, D.L. Stauff, B. Spiller, M.S. McClain, T.L. Cover, D.B. Lacy, Crystal structure of the Helicobacter pylori vacuolating toxin p55 domain, Proc. Natl. Acad. Sci. U.S.A. 104 (2007) 16293–16298, https://doi.org/10.1073/pnas.0707447104.
[41] H.A. Ahmed, M.A. El-Atawy, F.S. Alamro, N.S. Al-Kadhi, O.A. Alhaddad, A.Z. Omar, Mesomorphic, computational investigations and dyeing applications of laterally substituted dyes, Molecules 27 (2022) 8980.